Metal-Organic-Framework Derived Co-Pd Catalyst is Preferred over Fe-Pd for Reductive Upgrading of Furfural to Tetrahydrofurfuryl alcohol

Saikiran Pendem,[a,b] Bolla Srinivasa Rao,[a,b] David J. Morgan[c] Digambar B. Shinde,[d] Zhiping Lai,[d] Nakka Lingaiah,[a,b] and John Mondal*[a,b]

[a]Catalysis and fine chemicals Division, CSIR-Indian Institute of Chemical Technology, Uppal Road, Hyderabad-500007, India, Email:johncuchem@gmail.com, johnmondal@iict.res.in

[b]AcSIR-Indian Institute of Chemical Technology, Hyderabad-500007 (India)

[c]Cardiff Catalysis Institute, School of Cheistry, Cardiff University, Park Place, Cardiff, CF10 3AT. UK

[d]Division of Physical Science and Engineering, King Abdullah University of Science and Technology (KAUST), Thuwal 23955-6900, Saudi Arabia.

KEYWORDS: *N-doped carbon • Co_3O_4 • Fe_3O_4 • ZeoliticImidazolate Frameworks • Tetrahydrofurfuryl alcohol • Hydrogenation of furfural • Heterogeneous catalysis •*

ABSTRACT:

The function of palladium encapsulated nanohybrids with renewable platform molecules can be altered by bringing diversity in chemical compositions to step forward in bio-mass refining. In this respect we report $PdCo_3O_4$, $PdFe_3O_4$ nanoparticles encapsulated in a graphitic N-doped carbon matrix, to have a change in selectivity with superior catalytic activity for hydrogenation of biomass-derivedmoleculefurfural (FA). Under the optimized reaction conditions, newly designed $PdCo_3O_4$@NC catalyst was exhibited highly efficient catalytic performance in the hydrogenation of furfural to THFAL (Tetrahydrofurfuryl alcohol) compared with $PdFe_3O_4$@NC, providing 100% conversion of furfural with an exclusive yield of 95% for THFALand superior catalytic activity even up to four recycling tests. With the evidence of different characterization analysis data (XPS, H_2-TPR) of nanohybrid we can emphasise that the presence of PdCo-N_x active sites and the multiple synergistic effect between Co_3O_4 and Pd

(II), Co_3O_4 and Pd^0 as well as presence of N in the carbonaceous matrixis responsible for the superior catalytic activity and stability.

INTRODUCTION:

Currently, the modern world requires the sustainable production of biomass-derived chemicals such as fuels, fuel additives and value-added chemicals due to the diminishing of fossil feedstock reserves. Researchers have been focusing on finding sustainable ways to substitute fossil-derived feedstocks with residual biological matter such as crops, scrap wood, mill residuals, and other biomass resources.[1-4] In our present study, Furfural used as raw material to produce tetrahydrofurfuryl alcohol (THFAL), which is one of the typical chemical products derived from furfural and furfuryl alcohol (FAL). THFAL completely miscible with water and used as green solvent in agricultural and industrial applications, It can also be converted into to various chemicals such as 1,5-pentanediol (1,5-PeD) an important monomer in the plastics industry, 1-pentanol (1-PeOH), tetrahydropyran (THP), tetrahydro-2-pyranone (THP-2-one), methyl tetrahydrofuran, 2-pentanol, tetrahydrofuran, 1-butanol (1-BuOH), 1,2-pentanediol[5] and it is clearly pronouncing the importance of THFAL production. Salnikova *et al*. Reported selective hydrogenation of furfural to FAL using Pd/Fe_3O_4/HPS as a catalyst, the conversion of furfural was > 95% with selectivity for furfuryl alcohol > 94%. Whereas these processes required high pressure about 6.0 MPa.[6] Compared with Pd, Ru based catalysts show poor catalytic activity to hydrogenate C=C bonds in the aromatic ring of furfural.[7-9] Very recently, Rodríguez-Ramos *et al*. reported hydrogenation of furfural using a series of Ru-based catalysts under very mild conditions. Although conversion of furfural 93%, the selectivity toward total hydrogenation THFAL very poor.[8] Nowadays, Metal-organic frameworks (MOFs) derived nanostructural materials have been received enormous attention as a novel class of porous carbon materials by providing wide-range of various structural materials, especially in heterogeneous catalysis. MOFs have also been utilized in various research fields, such as energy storage,[10-12] supercapacitors,[13] gas separation,[14] oxygen reduction reactions,[15] CO_2 reduction,[16,17] oxidation reactions,[18] oxygen evolution reactions[19] and so on. And their efficient catalytic activity is due to the modifiable particle, pore sizes, controllable shapes,[18] and high specific surface areas with unique structures. Moreover, these materials are well known for developing N, P and S like hetero atom rich nanostructural carbon materials, and metal or metal oxide loaded porous carbons and N-doped porous carbons with novel

characteristics via pyrolysis process by acting as self-sacrificed template/precursor.[12,20-22] Introduction of nitrogen like heteroatoms into carbon materials decreases the charge transfer resistance to improve catalytic performance by a synergistic effect[20] between carbon and the heteroatom. 2-methylimidazole ligands of zeolitic imidazolate frameworks (ZIFs) are the unique source for developing carbon and nitrogen-rich (N-rich) MOFs derived porous nanostructural catalysts via direct carbonization.[22,23] Pd-3d transition metal oxides@N-dopedCarbon type catalysts are efficient for selective and total hydrogenation of biomass-derived furfural. The selectivity of hydrogenation of furfural can be varied with 3d transition metal oxides. In the present study, Pd-Fe_3O_4@NC tends to hydrogenate C=O functional groupoverfuron ring C=C bonds of furfural to produce furfuryl alcohol (FAL). FAL has been noticed as a valuable chemical compound with a wide range of applications such as foundry binders, precursors of resins.[24] Additionally, FAL can be used in the production of THFAL.[25] Interestingly, we noticed that the Pd-Co_3O_4@NC catalyst shown efficient catalytic activity towards hydrogenate furan aromatic ring C=C and C=O bonds of furfural with 100% yield with excellent catalyst durability and much higher activity with upto 4^{th} catalytic run indicates the good recyclability. Overally, it is pronouncing that the Co_3O_4 support is more effective for the total hydrogenation of furfural toproduce THFAL over Fe_3O_4 support. These Pd-Fe_3O_4 and Pd-Co_3O_4 decorated on porous nitrogen-doped carbon catalysts (Pd-Fe_3O_4@NC and Pd-Co_3O_4@NC) developed via direct thermal decomposition in H_2 flow of ZIF solid contain with an N-rich organic linker. The specific textural, chemical characteristics and atomic-level relationship between structure and catalysis of PdCo_3O_4@NC have been widely investigated by performing powder x-ray diffraction (P-XRD), high-resolution transmission electron microscopy (HR-TEM), scanning electron microscopy (SEM), temperature-programmed reduction (TPR), nitrogen adsorption-desorption, x-ray photoelectron spectroscopy (XPS) and Raman. On the basis of the detailed investigation with characteristic techniques, including H_2TPR and XPS, the active catalytic performance and durability of Pd-Co_3O_4@NC towards the hydrogenation of furfural to THFAL with 95% yield and good recyclability are can be attributed to the multipleintrinsic synergistic effect between Co_3O_4 and Pd(ＩＩ), Co_3O_4 and Pd^0 as well as presence of N. In other words, PdCo-N_x active sites in a carbonaceous matrix.

EXPERIMENTAL:

Catalyst Characterization:

Powder X-ray diffraction (PXRD) patterns of the different samples were recorded with a Bruker D8 Advance X-ray diffractometer operated at a voltage of 40 kV and a current of 40 mA using Ni-filtered Cu Kα (λ=0.15406 nm) radiation. High-resolution transmission electron microscopy (HR-TEM) images were recorded from a JEOL JEM 2010 transmission electron microscope with an operating voltage of 200 kV equipped with a field emission gun. Field emission scanning electron microscopy images of the samples were obtained using a JEOL JEM 6700 field emission scanning electron microscope (FE-SEM). Raman spectra of the samples were recorded using a LabRAM HR800 confocal microscope Raman system (HoribaJobin Yvon) with an Ar ion laser operating at 632 nm. Nitrogen sorption isotherms were measured at 77 K with an autosorbiQ automated gas sorption analyser (Quantachrome Instruments, USA). Before the measurements, the samples were degassed under vacuum at 200°C for 8 h. The Brunauer–Emmett–Teller (BET) method was utilized to determine the specific surface area using adsorption data in a relative pressure (P/P_0) range of 0.05–0.30. The total pore volumes and pore size distribution curves were obtained from the adsorption branches using the nonlocal density functional theory (NLDFT) method. X-ray photoelectron spectroscopy (XPS) was performed on aKratos Axis Ultra system using monochromatic Al Kα radiation, with a photon energy of 1486.6 eV. High resolution spectra were collected using a 20 eV pass energy, whilst survey spectra were collected at 160 eV, with step sizes of 0.1 and 1 eV respectively.. The H_2-TPR analysis was carried out in a quartz micro-reactor interfaced to a gas chromatograph (GC) equipped with a thermal conductivity detector (TCD) unit. Prior to TPR analysis, the catalyst was degassed at 300ºC in helium gas for 30 min and then cooled to room temperature. The helium gas was switched to 4.97% H_2 in argon with a flow rate of 30 mL min^{-1} and the temperature was increased to 900ºC at a ramping rate of 5ºC min^{-1}.

Catalyst Preparation:

Synthesis of stabilizedPd nanoparticles solution:

600 mg Polyvinylpyrrolidone (PVP) was dissolved in 180 mL methanol then Palladium acetate trimmer solution (80 mg Palladium acetate trimmer dissolved in 6.2 mL H_2O) was slowly added with continuous stirring at room temperature, after that this mixture was refluxed at 70°C in air for 3 h, resulting mixture was dried using rota evaporation, obtained black solid Pd stabilized nanoparticles material was dissolved in 50 mL H_2O.

Metal-Organic-Framework derived synthesis of Pd-Fe_3O_4& Pd-Co_3O_4 nanoparticles on N-Doped Porous Carbon Sheets:

2-methylimidazole (1.312g) and PVP (0.08g) was dissolved in 100 mL methanol, then this solution was slowly added into metal nitrate solution ($Co(NO_3)_2.6H_2O$ (4 mmol, 1.164g) dissolved in 100 mL methanol) with continuous stirring at room temperature, after that stabilised Pd nanoparticles solution (16 mL) was slowly dropwise added into previous solution and stirred for 45 minutes at room temperature, resulting mixture was supposed to age for 24 h, obtained solution was washed several times with methanol using centrifugation and dried in air, and then this solid material was heated at 120°C (10°C min^{-1}) for 1 h then 300°C (10°C min^{-1}) for 2 h in H_2 flow. The obtained solid component was assigned as Pd-Co_3O_4@NCsheets. Pd-Fe@NC was also prepared using the same synthesis process, the obtained component using $Fe(NO_3)_3.9H_2O$ ($Fe(NO_3)_3.9H_2O$ (4 mmol, 1.616g) dissolved in 100 mL methanol) as metal nitrate solution in the above procedure assigned as Pd-Fe_3O_4@NC.

Activity Test:

All the hydrogenation reactions of furfural were performed in a stainless-steel Parr autoclave inbuilt with a 190 pressure gauge setup lined with Teflon (50 mL), for a typical hydrogenation of furfural, 50 mL Parr autoclave was charged with a mixture of furfural (1 mmol), isopropanol (25 mL), 70 mg catalyst and the reactor was sealed with an overhead stirrer and purged four times with molecular hydrogen (H_2). Then the reactor was pressurized with H_2 (20 bar) and heated at 150°C with stirring at a speed of 700 rpm for 6 h. Then the reactor was stopped and the pressure in the autoclave was slowly released after the reactor cooled to room temperature. The solid catalyst was recovered from the reaction mixture by centrifugation and the isolated liquid reaction mixture was analyzed by chromatography (GC). GC (Shimadzu 2010) equipped contain with a flame ionization 200 detector (FID), no wax capillary column (length: 30 201 m diameter: 0.25 mm), and gas chromatography-mass spectrometry (GC-MS) (Shimadzu, 202 GCMS-QP2010S) were utilized for quantitative analysis and product detection in the presence of 1,4-dichlorobenzene as an internal standard. In the GC and GC-MS analysis, the initial column temperature of 50°C was held for 2 min, after that the temperature was programmed as 100°C with a ramprate of 5°C m^{-1} and held for 2 min, again the temperature was ramped at 10°C m^{-1} until 250°C was reached and held for 2 min. in addition, the injector, detector temperatures were fixed to 250°C and 270°C, respectively.

Hot Filtration Test:

In order to confirm the heterogeneous and robust nature of our newly developed PdCo_3O_4@NC nanohybrid we have conducted a hot filtration test in a 50 mL Parr autoclave charged with a

mixture of furfural (1 mmol), isopropanol (25 mL), 70 mg catalyst and the reactor was sealed with an overhead stirrer and pressurized with H_2 (20 bar) and heated at 150°C with stirring at a speed of 700 rpm for 2 h. After reaction proceeded for 2 h, the catalyst was isolated from the hot reaction mixture by centrifugation and sample prepared from filtrate for GC analysis, 100% furfural conversion with 75% yield was noticed over $PdCo_3O_4$@NC, then we have performed same catalytic reaction at identical reaction conditions with collected filtrate for an additional 6 h, and no considerable hydrogenation of filtrate was noticed by GC analysis indicating that there is no leaching of nanoparticles due to nanoparticles strongly anchored with N-doped carbon matrix pronouncing the robust nature of $PdCo_3O_4$@NC.

RESULTS AND DISCUSSION:

The successful development of robust hollow structured $PdCo_3O_4$@NC nanohybrid was achieved in a systematic and easy catalyst preparation strategy as illustrated in Scheme 1. Initially, PVP-Pd@ZIF-67 composite was developed by consuming 2-methylimidazole as a self-sacrificed template, $Co(NO_3)_2.6H_2O$ and Palladium acetate trimmer involved as a metal source at room temperature, in the overall synthesis process PVP served as a stabilizer in Pd nanoparticle synthesis and developing nanocomposite. The deep washing of prepared composite with methanol removes the molecules loosely adsorbed on PVP-Pd@ZIF-67 composite through electrostatic interactions. The characteristic FE-SEM of the solid nanocomposite of PVP-Pd@ZIF-67 shown in Figure S1 ESI. As final step solid PVP-Pd@ZIF-67 was pyrolyzed under the molecular hydrogen gas flow at pre-programed-temperature (120°C, 10°C min^{-1} than 300°C, 10°C min^{-1}) to obtain Pd-Co_3O_4 encapsulate in graphitic N-doped carbon matrix denoted as $PdCo_3O_4$@NC. During the decomposition of nanocomposite, the organic ligands from the ZIF are condensed to form nitrogen doped porous carbon matrix, on other side the formation of Co_3O_4 begins as raising temperature to 300^0 C from Co^{2+} which further interact with Pd to produce Pd-Co_3O_4, which were in situ confined into N-doped carbon matrix, leading to homogeneous dispersion of the Pd-Co_3O_4 on carbon matrix with controlled generation of highly catalytically PdCo-N_x active sites with an effective approach for graphitization of amorphous carbon by solid-state transformation method.

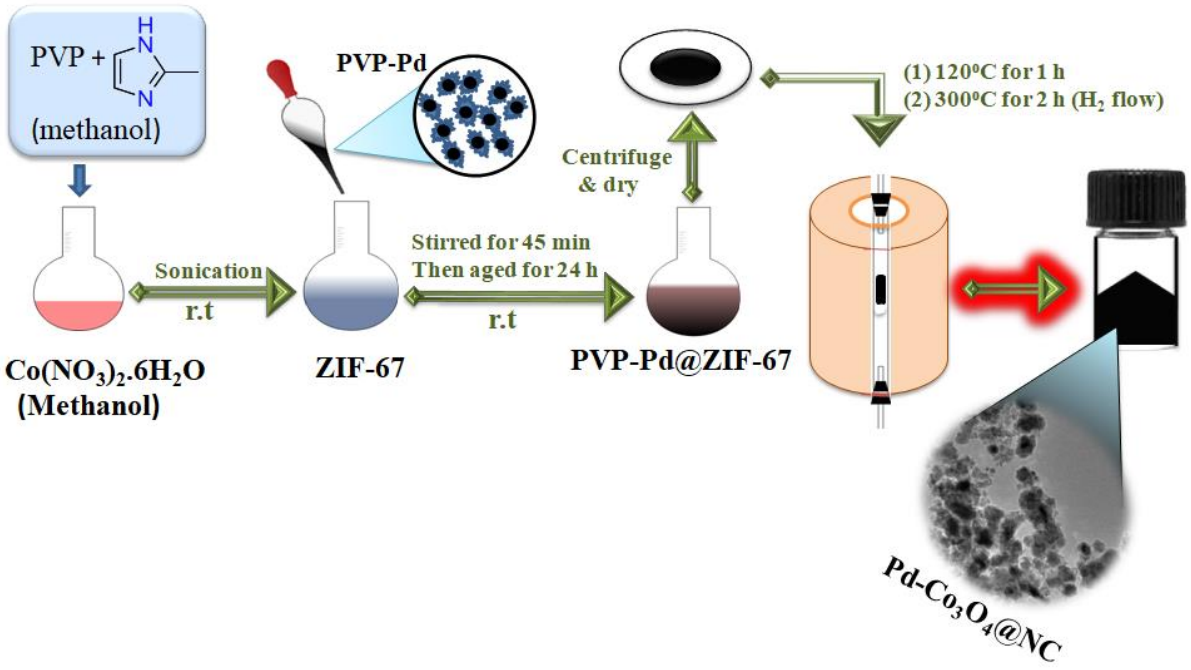

Scheme 1: Schematic illustration for metal-organic-framework mediated synthesis of Pd-Fe_3O_4 & Pd-Co_3O_4 nanoparticles on N-doped porous carbon sheets

The formation of Co_3O_4 and Fe_3O_4 confirmed by the X-ray diffraction analysis of the prepared samples, the X-ray diffractograms were scanned between wide angles of 5-80° (2θ). Pd-Fe_3O_4@NC sample exhibited six peaks, the absence of other phases of iron oxide, characteristic for the magnetic cubic structure of Fe_3O_4 (Figure 1) phase at 2θ values of 30.3°, 35.7°, 43.3°, 54.1°, 57.4° and 62.9° (JCPDS 19-0629) with the corresponding diffraction planes of (220), (311), (400), (422), (511) and (440).[26] There is no noticeable Pd (0) diffraction peak for both Pd-Fe_3O_4@NC and Pd-Co_3O_4@NC indicative of finely dispersed Pd (0) and its existence confirmed by XPS analysis (figure 4) and H_2-TPR (figure 3). Pd- Co_3O_4@NC exhibited characteristic peaks of Co_3O_4 phase at 2θ values of 36.6° and 44.5° (JCPDS-ICDD 9-418) with the corresponding to the (311) and (400) diffraction planes indicating the successful formation of high crystalline quality metal oxide (Co_3O_4) (Figure 2).[27] Surface properties of catalysts could be determined using Nitrogen adsorption-desorption isotherm. The obtained isotherm of both PdFe_3O_4@NC and PdCo_3O_4@NC catalysts are corresponding to a type (II) with H3 hysteresis in the Brunauer classification confirms the existence of inter-particle void spaces, and it does not show any limiting adsorption at high relative pressures (P/P_0). The Brunauer-Emmett-Teller surface area (S_{BET}) for Pd-Fe_3O_4@NC and Pd-Co_3O_4@NC was found to be 60.96m^2/g and 109.07m^2/g, respectively.The pore size distribution of PdCo_3O_4@NC was measured to be 1.70nm, which further confirms its microporous nanostructure. Interestingly, a comparable pore size distribution centered at 1.70 for PdFe_3O_4@NC due to similar dense

nanoparticles serves as templates to generate microporous N-doped carbon nanostructure in both catalysts, and the additional pores, which are formed from uncontrolled aggregated nanoparticles of Fe-ZIFs thermal treatment in H_2 flow, were noticed from $PdFe_3O_4$@NC as well. (Figures S2, S3, ESI).

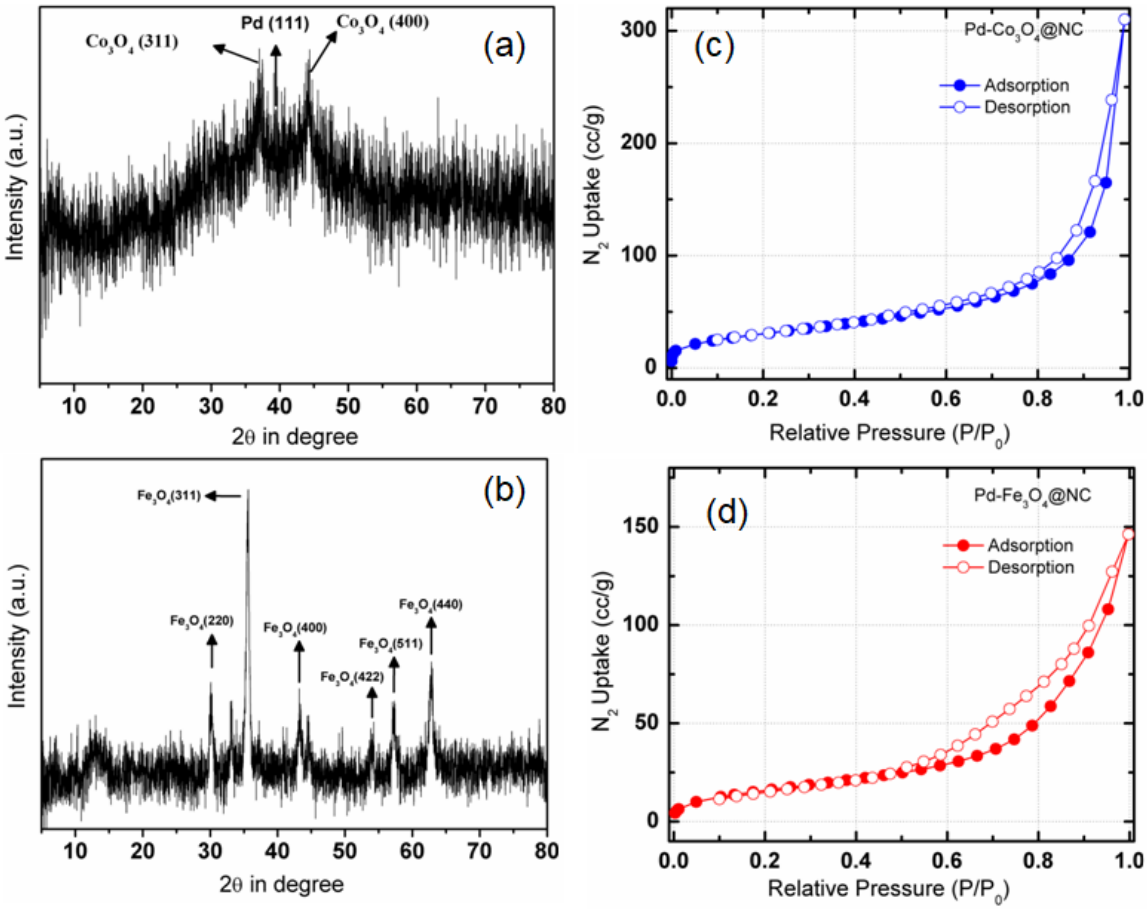

Figure 1: Wide angle power XRD patterns (a) and (b), N_2 adsorption/desorption isotherms (c) and (d), of Pd-Co_3O_4@NC and Pd-Fe_3O_4@NC, respectively.

Nanostructures, Particle size and morphology of Pd-Fe_3O_4@NC and Pd-Co_3O_4@NC composites evidently studied by high-resolution transmission electron microscopy (HR-TEM), transmission electron microscopy (TEM) and scanning electron microscopy (SEM) analytical techniques. The morphology of Pd-Fe_3O_4@NC and Pd-Co_3O_4@NC is clearly categorized by the FE-SEM images (Figure S5 ESI).As presented in Figure S5b ESI, The closely packed Pd-Fe_3O_4 nanoparticles decorated on N-doped carbon flake type sheets, which could also be clearly seen from TEM images that well-defined and homogenous spherical shape of nanoparticles. But in the case of the Pd-Co_3O_4@NC compound consistency of closely packed spherical shape of particles very clearly noticed from SEM images (Figure S5a ESI). Actually, Pd-Fe_3O_4 nanoparticles tend to form aggregates due to high surface energy, and high surface interaction

between the nanoparticles and large specific surface area. In the TEM images (Figure 2), uniformly distributed darker spots of spherical metal oxides nanoparticles surrounded by lighter regions of n-doped carbon matrix in Pd-Fe_3O_4@NC and Pd-Co_3O_4@NC are developed by aggregation process of metal oxides nanoparticles with an average size range of 11.9-21.8 (Fe_3O_4) and 20-40 nm (Co_3O_4). As shown in Figure 2b & 2d, HR-TEM images along withthe corresponding Elemental mapping data are clearly representing the hollow metal oxide (Co_3O_4, Fe_3O_4) polycrystals, the distinguished crystalline lattice spacing about 0.30nm attributed to (220) diffraction planes omitted from crystallographic planes of the inverse spinel Fe_3O_4 nanoparticles. Parallel fringes having d-spacing of ~0.204 and 0.248nm, respectively are corresponding to the (400) and (311) diffraction planes of the normal spinel Co_3O_4 nanoparticles which is similar to powder XRD crystalline reflections. Moreover, the corresponding high angle annular dark field scanning transmission electron microscopy Elemental mapping data of nanohybrids further confirmed the homogeneous distribution of elements O, C, Pd and Co of Pd-Co_3O_4@NC, and O, N, C, Pd and Fe of Pd-Fe_3O_4@NC on the catalyst surface, respectively.

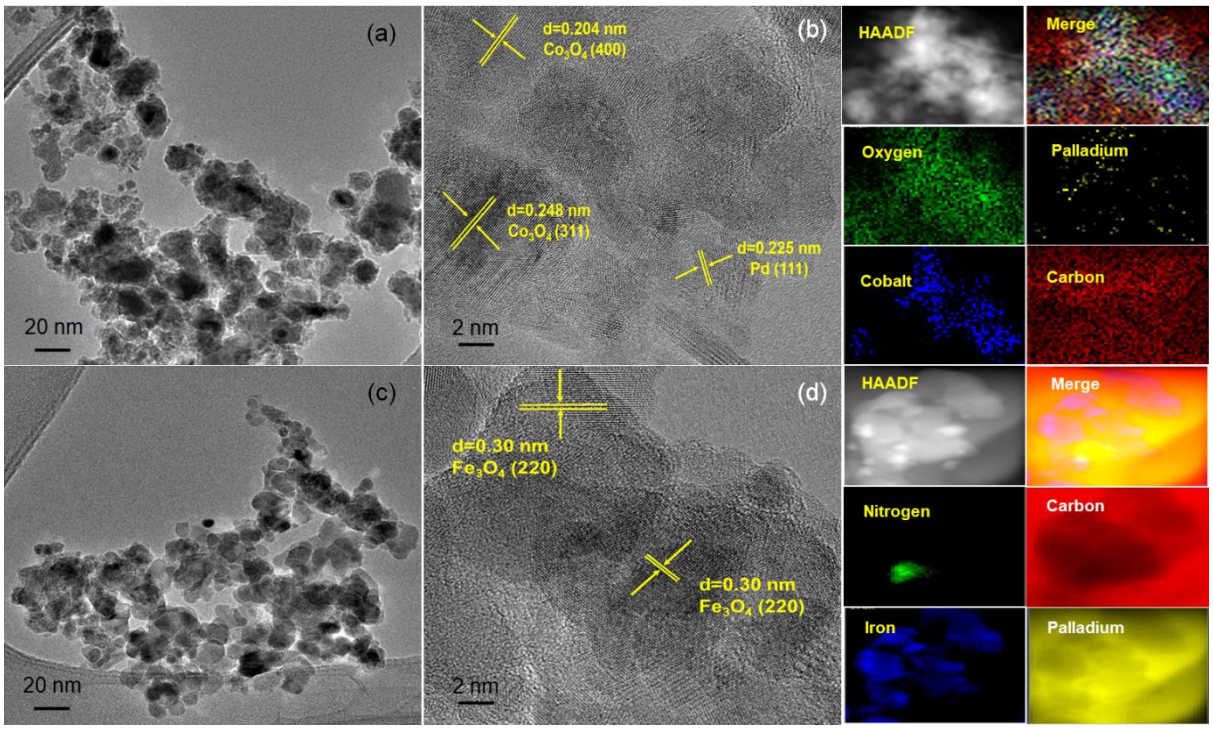

Figure 2:HR-TEM images (a & b) of Pd-Co_3O_4@NC, (c & d) of Pd-Fe_3O_4@NC, respectively with corresponding Elemental mapping data.

As shown in Figure 3, the H_2-TPR of Pd-Fe_3O_4@NC and Pd-Co_3O_4@NC is indicating the successful loading of palladium, and the formation of Fe_3O_4 and Co_3O_4, respectively. The H_2-TPR of Pd-Fe_3O_4@NC exhibited a peak about 120-207cm^{-1} corresponding to the reduction of Pd-O to Pd, and a broad peak appeared at 470-840 cm^{-1} is due to overlapping of Fe_3O_4 to FeO peak at 420-660 cm^{-1} and FeO to Fe peak at 660-850 cm^{-1} revealing the consistency of Fe_3O_4 phase.[28] Usually, the discrepancy in chemical states of Pd nanoparticles directs to deferent redox properties. The Pd-Co_3O_4@NC exhibited a broad reduction peak of Pd(II) to Pd at 104-315 cm^{-1} with slow uptake by consuming H_2 continuously is due to inhibition of in-situ formation of PdO via lowering the reduction temperature of Pd-O to Pd by Co_3O_4. Interestingly, Pd(II) reduction temperature shifted towards higher temperature indicating the stabilization of Pd(II) due to the formation of Pd-O-Co bond between Pd(II) and Co_3O_4,[29] and it is pronouncing that the existence of electronic interaction between Pd and Co. The broad peak and a small peak at 299-600 cm^{-1} is due to two-step reduction process of Co_3O_4, the first peak is due to Co_3O_4 to CoO reduction and the second peak is due to the subsequent reduction of CoO to Co.

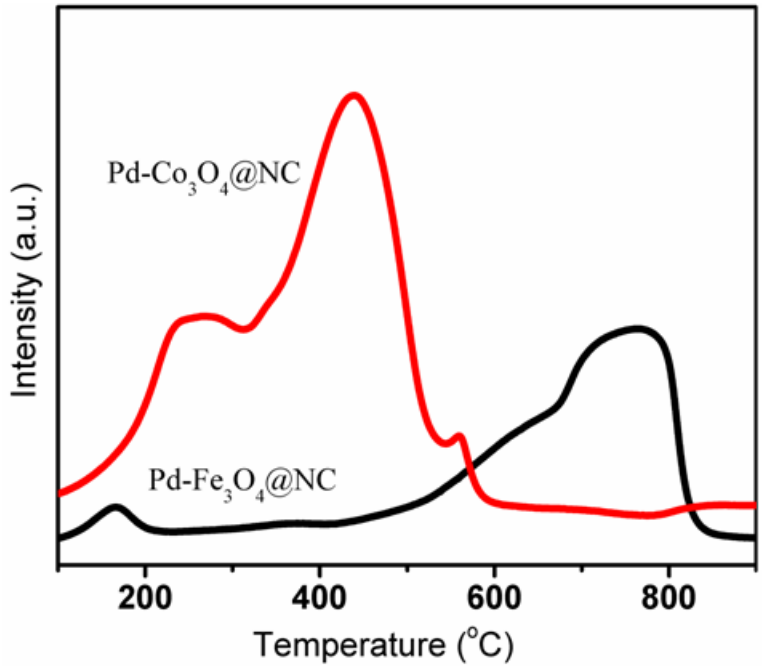

Figure 3: H_2-TPR profiles of Pd-Co_3O_4@NC & Pd-Fe_3O_4@NC, respectively.

The electronic structure and chemical state of Pd nanoparticles in Pd-Co_3O_4@NC and Pd-Fe_3O_4@NC catalysts, and surface electronic property and elemental compositions were evidently identified by XPS investigation of Pd-3d, Co-2p, Fe-2p and N1s of Pd-Co_3O_4@NC

and Pd-Fe_3O_4@NC (Figure 4) at their corresponding binding energies. The N-1s XPS spectrum of Pd-Co_3O_4@NC exhibited a broad peak which could be resolved in to two components attributed to pyridinic N at 399.1 eV and graphitic N at 400.4 eV. The pyridinic N peak resulted from Pd-Co_3O_4@NC shifted towards the high binding energy about ~0.3 eV compared with Pd-Fe_3O_4@NC revealing that the pyridinic N (Lewis base) strong interactions with Co_3O_4 confirming the successful formation of the N-doped carbon matrix and it is well known that the synergistic effect between Pd and N play additional role in enhancing the catalytic activity.[30,31] whereas, in Pd-Fe_3O_4@NC the N-1s binding energy of pyridinic N located at 398.8 eV (Figure 4d). As shown in Figure 4a, the Pd-3d XPS spectra of PdCo_3O_4@NC exhibited a sharp doublet with the $3d_{5/2}$ peak centred at 335.3 eV w corresponding to Pd^0 (Figure 4a). Interactions between Pd^0 and Co_3O_4 can be attributed to intrinsic synergistic effect developed by charge transfer of electrons between Pd and Co,[30]and shown enhanced activity in the hydrogenation of furfural, and one more doublet with a Pd5/2 peak at 338.0eV corresponding to Pd(II) which connected with Co_3O_4.[32] Moreover, we also identified that the electronic structural properties of Co_3O_4 in PdCo_3O_4@NC nanohybrid is quite similar to those investigated by Xihong Lu *et al.* The investigation of Co-2p XPS spectra at binding energy of 779.6 eV revealing (Figure 4c) that as lattice oxygen atoms containing Co_3O_4 (O 1s, Figure S4 ESI) interacting with Pd(II) nanoparticles the Lewis acidic nature of Co_3O_4 enhances due to synergistic effect between Co_3O_4 and Pd(II) by electron transport from Co_3O_4 to Pd(II), and it pay a key role in favoring the interactions between carbonyl group of furfural with Co_3O_4 to succeed coordination bond as well in hydrogenation process in presence of Pd^0 via hydrogen dissociation and spillover on Co oxide encapsulated in graphitic N-doped carbon matrix.[33,34] In the case of the Pd-Fe_3O_4@NC catalyst Pd-3d XPS spectra exhibited metallic Pd as indicated by the 3d5/2 signal at, 334.9 eV this bulk like value suggests that either the particles are bigger, exhibiting more bilk like properties, or there is littleconsiderable interactions between Pd and Fe_3O_4 lowers the charge transport between the Pd and Fe_3O_4 which can be suppress the capability of ring hydrogenation of furfural,and the second one at lower binding energies compare with Pd-Co_3O_4, binding energy of 337.2eV indicating the existence of Pd(II). The Fe 2p XPS spectra indicates no other iron oxides are present, with the $Fe2_{p3/2}$ peak at 710 (Fe 2p3/2), along with satellite peaks can attributed to the magnetite (Fe_3O_4) (Figure 4b).[35]

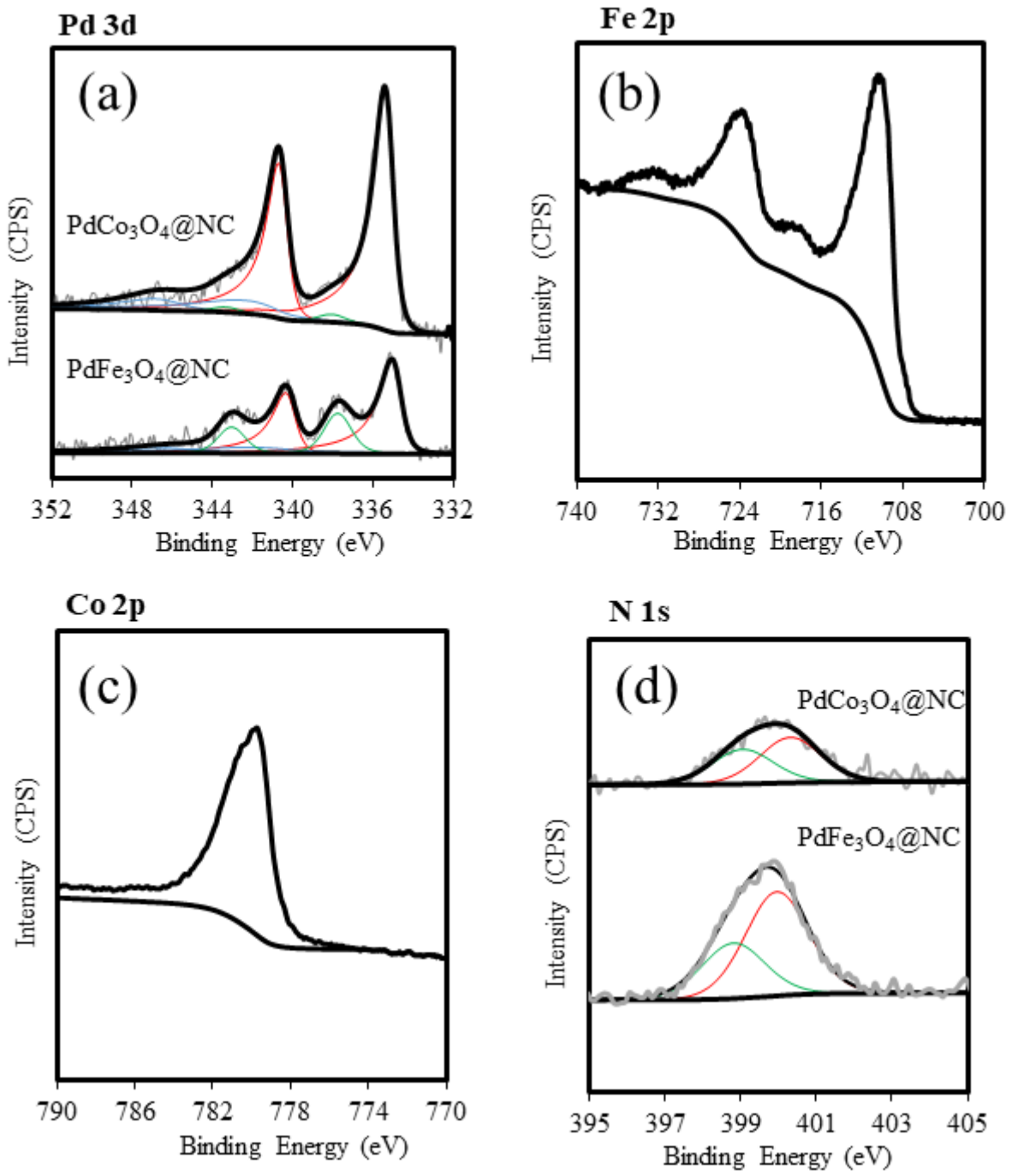

XPS: Figure 4: Fitted Pd-3d (a), Fe-2p (b), Co-2p (c), N-1s (d), XP spectra of$Pd\text{-}Fe_3O_4@NC$ & $Pd\text{-}Co_3O_4@NC$, respectively.

In addition to powder XRD the formation of Co_3O_4 and Fe_3O_4 phases is confirmed by the Raman spectroscopy analysis of untainted $Pd\text{-}Fe_3O_4@NC$ and $Pd\text{-}Co_3O_4@NC$ catalysts. The Raman spectra of $Pd\text{-}Fe_3O_4@NC$ exhibited one broadband around 660 cm^{-1} corresponding to A1g mode and two broadbands around 1359 and 1583 cm^{-1} areattributed to the vibration modes of Fe_3O_4 phase and hematite, respectively.[36,37] As space group theory predict Γ=A1g + Eg +

3F2g vibration modes are Raman active modes as "Fd3m" symmetry for the Co_3O_4 normal spinel configuration, the Pd- Co_3O_4@NCnanoparticles exhibited five characteristic bands around 197, 484, 524, 621 and 690 cm^{-1} can be attributed to Raman active F2g, Eg, 2F2g and A1g vibration modes of normal spinel Co_3O_4 phase, respectively (Figure 5). Out of five Raman active vibrational modes, the F2g (197 cm^{-1}) vibration mode corresponding to CoO_6 scissoring vibration mode, whereas Eg (484 cm^{-1}), 2F2g (524, 621 cm^{-1}) and A1g (690 cm^{-1}) are exhibit Co-O symmetric stretching vibration.[38-40]

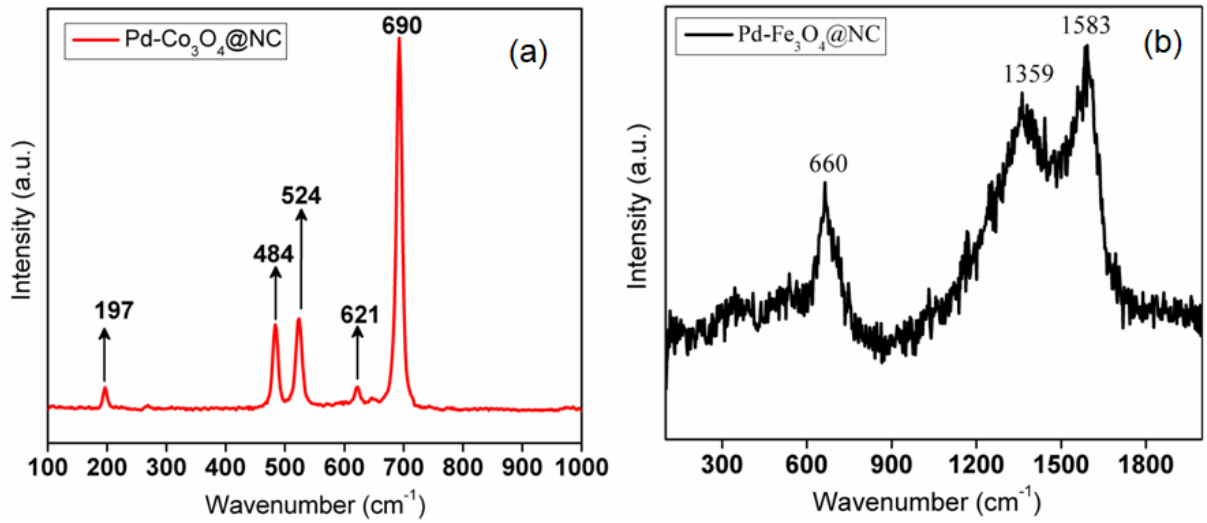

Figure 5: Raman spectra of Pd-Co_3O_4@NC (a) & Pd-Fe_3O_4@NC (b), respectively.

Catalytic activity for reductive upgrading of bio-mass derived furfural:

To evaluate the catalytic activity of the as-synthesized PdCo_3O_4@NC we have conducted Hydrogenation of furfural. During the course of the reaction, we have noticed the formation of the verity of products from furfural over the PdFe_3O_4@NC and PdCo_3O_4@NC catalyst (Scheme S1 ESI). The formation of THFAL from furfural involves two subsequent steps. hydrogenating furan aromatic ring C=C is hard compared with C=O bonds of furfural as presented in plausible mechanism Scheme S1 ESI, in the first step furfural interact with a catalyst to produce furfuryl alcohol (FAL), subsequently, second step initiate to hydrogenate furon ring of furfuryl alcohol to yield desired THFAL. Further THFAL interaction with metal involves in hydrogenolysis process to yield MeTHF which is a by-product of furfural hydrogenation using PdFe_3O_4@NC and PdCo_3O_4@NC as a catalyst. Our catalytic study experiments evidently proved the plausible mechanism. The beginning of catalytic activity study is the comparison, and the effect of reaction time, temperature and pressure on the catalytic activity of PdFe_3O_4@NCand PdCo_3O_4@NC (Figure 6). As shown in Figure 6b in

presence of $PdFe_3O_4$@NC, at initial 1 h time period the product yield of THFAL, FAL noticed as 28% and 71%, respectivelyalong with the formation of side products (MeTHF, 2-Methylfuron) with 100% conversion. Herein we noticed that the THFAL yield further enhanced to 70% by hydrogenating FAL to THFAL as expanded the time period to 8 h at identical 20 bar H_2, 150°C. Interestingly, the $PdCo_3O_4$@NC nanohybrid was exhibited complete conversion of furfural with the 60% yield of THFAL and 33% yield of FAL at reaction time period for 1 h. As increasing the reaction time period 1 h to 8 h during the optimization of reaction time at fixed H_2 pressure (25 bar) and temperature (150°C) gradual increase in the product yield of THFAL with the maximum of 95% up to 6 h noticed which indicating that the active sites are initially engaged in interacting with furfural carbonyl group Pd(II) in presence of Pd^0 to yield FAL which subsequently undergoes to produce THFAL due to the total hydrogenation of furfural to THFAL proceeds via hydrogenating C=O and furan aromatic ring C=C bonds of furfural, respectively, the C=O bond is less stable and easy to hydrogenate than furan aromatic ring C=C bonds (Scheme S2 ESI)[41,42] and the further extension of time period to 8 h declined the THFAL yield to 88% which can be ascribed to the hydrodeoxygenation of THFAL into undesired side product methyl tetrahydrofuran (MeTHF) in presence of $PdCo_3O_4$@NC with the complete conversion as well (Figure 6a).

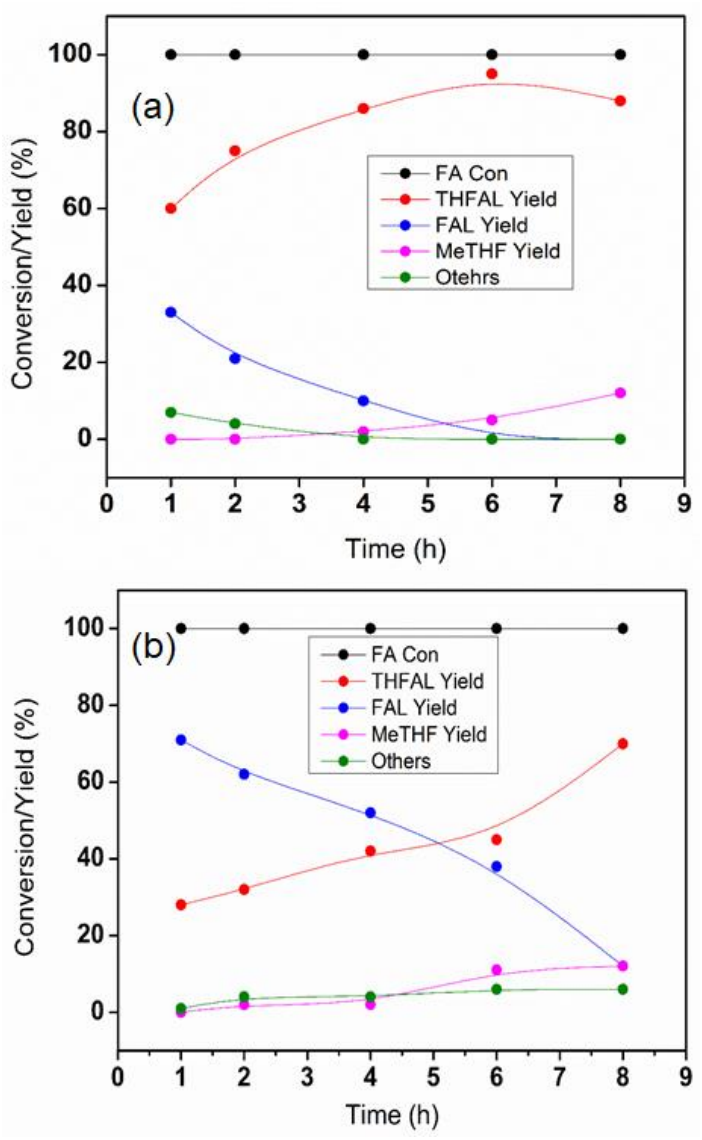

Figure 6: Evolution of reactant and product distributions as a function of time over (a) $PdCo_3O_4$@NC, (b) $PdFe_3O_4$@NC. Reaction conditions: furfural (1 mmol), isopropanol (25 mL), 70 mg catalyst, H_2 (20 bar), 150°C.

A similar scenario has been identified while investigating temperature and pressure influence on the catalytic activity of both catalysts, the desired product yield of THFAL and the side products yield affected as well. As the temperature increase 90 to 200°C at the fixed H_2 pressure of 20 bar, the maximum product yield of THFAL with 95% achieved at 150°C for $PdCo_3O_4$@NC and quite dissimilar from $PdFe_3O_4$@NC further increase of temperature from this point the continuous decline in product yield of THFAL observed on another side MeTHF percentage of yield gradually increased to 41% via hydrodeoxygenation process at high temperature (220°C) (Figure 7c),. High product yield (88%) of FAL has been noticed in presence of $PdFe_3O_4$@NC at lower temperatures (90°C), and as raising the temperature from lower to higher (200°C) the yield of THFAL reached 65%, further involved in the

hydrogenolysis process to yield MeTHF at 220°C (Figure 7d). Eventually, after an investigation of temperature effecton the catalytic activity of catalysts, the pressure influence of H_2 pressure ranging from 15-30 bar has been examined. With increasing the H_2 pressure from 15-25 bar, the required abundance of dissolved H_2in the reaction mixture was achieved at 25 bar and obtained the huge yield of THFAL with 95% at 150°C and 6 h reaction time period for $PdCo_3O_4$@NC (Figure 7a). In presence of $PdFe_3O_4$@NC furfural converted into FAL with 71% product yield at an initial H_2 pressure of 15 bar and the maximum yield of THFAL noticed at 30 bar due to further hydrogenation of FAL at high pressure (H_2 30 bar) (Figure 7b).

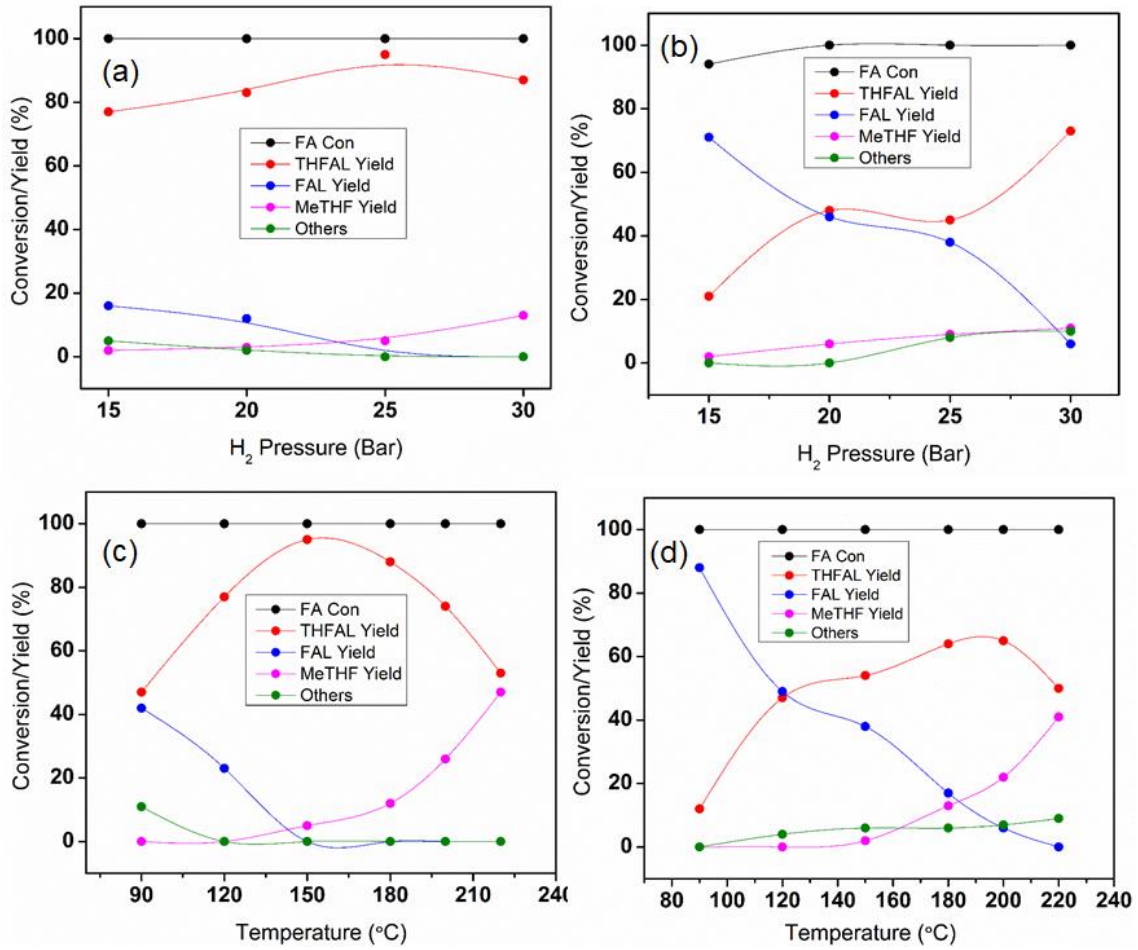

Figure 7: Influence of H_2 pressure (a & b) & temperature (c & d) on $PdCo_3O_4$@NC & $PdFe_3O_4$@NC, respectively. Reaction conditions: furfural (1 mmol), isopropanol (25 mL), 70 mg catalyst, H_2 (20 bar), 6 h.

In order to evaluate the superior catalytic activity of $PdCo_3O_4$@NC towards the hydrogenation of furfural to THFAL, we have compared reported Pd-Based Catalysts catalytic activity for conversion of furfural to THFAL (Table S1 ESI), additionally, we have developed a series of catalysts including CuFe@NC, CuCo@NC, Co@NC and Fe@NC by following a similar

synthesis procedure involved in the development of $PdCo_3O_4$@NC nanohybrid. From the comparison study as depicted in Figure 8 we have achieved 100%, 100%, 38%, 23% furfural conversion from CuFe@NC, CuCo@NC, Co@NC and Fe@NC, respectively, at optimized reaction conditions. Especially the yields of THFAL from furfural for corresponding catalysts are noticed as very low compared with $PdCo_3O_4$@NC . Fe@NC, Co@NC provided much lower yields of THFAL 3% and 12%, respectively. CuFe@NC and CuCo@NC catalysts exhibited improved catalytic activity and the yields of THFA are 27% and 42%, respectively, with complete conversion of furfural Which conclude that the Cu promoted Co/Fe and Co/Fe are less active in N-doped carbon matrix to achieve desired product THFAL suggesting the importance of enhanced Lewis acidic nature of Co_3O_4 by synergistic effect between Co_3O_4 and Pd(II) in PdCo-N_x active sites to achieve the interactions between carbonyl group of furfural with metal oxide in hydrogenation process of furfural. But in the case of $PdFe_3O_4$@NC exhibited considerably good yields at first reaction run (45%, 6 h) although which is unstable indicating the impact of Pd^0 in achieving enhanced THFAL yields. As a final step in the comparison study, we have conducted the hydrogenation reaction of furfural in inert conditions too for $PdCo_3O_4$@NC and $PdFe_3O_4$@NC, and the resulted yields of THFA are 35% and 45%, respectively (Figure 8). However, from comparison investigation conclude that the $PdCo_3O_4$@NC nanohybrid exhibited superior catalytic activity with exclusive yields of THFA (95%) (Figure 6a).

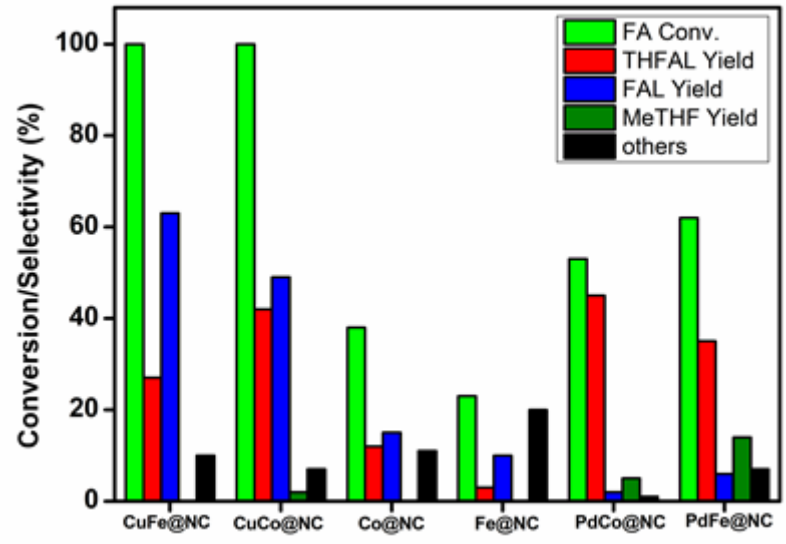

Figure 8: Reaction conditions: furfural (1 mmol), isopropanol (25 mL), 70 mg catalyst, H_2 (20 bar), 6 h for CuFe@NC, CuCo@NC, Co@NC and Fe@NC. furfural (1 mmol), isopropanol (25 mL), 70 mg catalyst, inert atmosphere, 6 h for PdCo@NC and PdFe@NC.

In order to affirm the stability of catalyst, we have done XPS analysisat 3d-Pd region of used catalysts along with reusability test as well. Interestingly, we noticed that the $PdCo_3O_4$@NC nanohybrid exhibited a sharp doublet with high intensity similar with fresh catalyst at the binding energy of ~340.5 and ~335.4 eV corresponding to the Pd^0 interacted with Co_3O_4further confirming the negligible leaching of Pd and the robust nature of Pd-Co_3O_4@NC nanohybrid, additionally, these results well consistent with the hot filtration test. Whereas Pd-3d XPS spectra of $PdFe_3O_4$@NC (Figure 10a) very clearly indicating the huge amount of leaching of Pd from the catalyst due to the existence of Pd in the form of bulk Pd(0) ($3d_{3/2}$ = 40.2 eV; $3d_{5/2}$ = 334.9 eV) which is loosely binded on Fe_3O_4@NC surface with less interactions between Pd and Fe_3O_4 diminishes the stability of catalyst. The Fe 2p XPS spectra peaks of used catalyst noticed at the binding energies about 710.3 (Fe 2p3/2), 724.152 (Fe 2p1/2) along with satellite peaks (Figure S6 ESI), and identical with fresh catalyst Fe 2p XPS spectra.Moreover, the elemental surface composition of carbon noticed as 55.36 and 59.02 mol % for used $PdCo_3O_4$@NC and $PdFe_3O_4$@NC catalysts, respectively, indicating that there is more amount of carbon deposited on the surface of the used $PdFe_3O_4$@NC catalystcompared to the used $PdCo_3O_4$@NC catalyst, and very poor signal detection noticed from used $PdFe_3O_4$@NC catalyst. The obtained result from XPS analysis of fresh and used catalystssuggested that the stability of active $PdCo_3O_4$@NC nanohybrid improved which could be ascribed to the strong synergistic effect between Pd and Co_3O_4 compared with Pd and Fe_3O_4. Moreover, we have noticed good results from reusabilitytest up to fourth reaction run (Figure 10b) which furtherly confirmed the robust nature of $PdCo_3O_4$@NC nanohybrid. After isolation of $PdCo_3O_4$@NC nanohybrid by centrifugation followed by washed with the methanol and oven dried at 80ºC from the first run reaction mixture we have conducted four more reaction runs at optimized reaction conditions and the yields of THFAL from furfural obtained as 94, 92, 89 and 85% for second, third, fourth and fifth run, respectively, with complete conversion, and this negligible decline in the yield of THFAL can be attributed to minimal carbon deposition on the surface of the active sites which may furtherly lead to the minimized porosity of nanohybrid.[43,44]

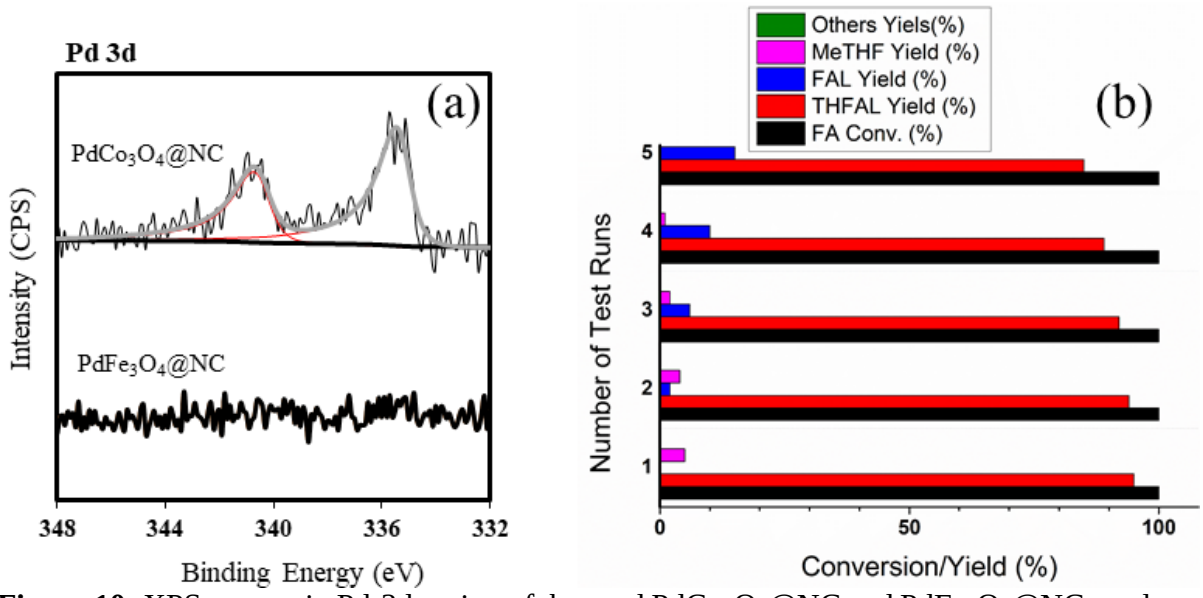

Figure 10: XPS spectra in Pd-3d region of the used $PdCo_3O_4$@NC and $PdFe_3O_4$@NC catalysts (a), investigation of the stability of the catalyst. Experimental conditions: furfural (1 mmol), isopropanol (25 mL), 70 mg catalyst, H_2 (20 bar), 6 h (b).

CONCLUSIONS:

In summary, present study describes the facile strategy to development of $PdCo_3O_4$ nanoparticles encapsulated in graphitic N-doped carbon matrix ($PdCo_3O_4$@NC), via stabilized Pd nanoparticle (PVP-Pd) deposited on the ZIFs metal-organic framework (PVP-Pd@ZIF-67) subsequently pyrolyzed in molecular hydrogen gas, for deep insight into investigation and comparison with $PdFe_3O_4$@NC synergetic effects on catalytic activity. In particular, $PdCo_3O_4$@NC nanohybrid with a composition of $PdFe_3O_4$@NC exhibited superior catalytic activity toward the conversion of furfural 100% with an exclusive yield 95% for hydrogenation product THFAL (Tetrahydrofurfuryl alcohol). The characterization techniques including XPS (fresh and used catalysts), H_2-TPR studies experimentally evidenced that the presence of PdCo-N_x active sites and the multiple synergistic effects are responsible for the superior catalytic activity and stability of $PdCo_3O_4$@NC nanohybrid.

ASSOCIATED CONTENT

†Electronic supplementary information (ESI) available: Characterization techniques,Pore-size distribution, FE-SEM images & O-1s XPS spectra of $PdCo_3O_4$@NC and $PdFe_3O_4$@NC, FE-SEM images of PVP-Pd@ZIF-67 and Proposed mechanistic pathway for catalytic hydrogenation of furfural to THFAL

AUTHOR INFORMATION

Corresponding Authors

*E-mail: johncuchem@gmail.com, johnmondal@iict.res.in

ORCID

John Mondal: 0000-0001-7813-2108

Notes

The authors declare no competing financial interest

ACKNOWLEDGMENTS

The authors are grateful for the financial support by the Department of Science and Technology, India, for DST-INSPIRE Faculty Research project grant (GAP-0522) at CSIR-IICT, Hyderabad. P.S. wishes to thankfully acknowledge CSIR, New Delhi, for his respective CSIR-UGC fellowship.

REFERENCES:

1. I. Ganguly, F. Pierobon, T. C. Bowers, M. Huisenga, G. Johnston, I. L. Eastin, *Biomass and Bioenergy.* **2018,** *108,* 207-216.
2. K. Dutta, A. Daverey, J. G. Lin, *Renew. Energy.* **2014**, *69*, 114-122.
3. P. Champagne, *Resour Conserv Recycl.* **2007**, *50*, 211-230.
4. M. Alkasrawi, Z. Al-Hamamre, M. Al-Shannag, M. J. Abedin, E. Singsaas, *Bio Res.* **2016**, *11*(1), 2287-2296.
5. C. Wang, J. D. Lee, Y. J. T. Ming Onn, J. Luo, C. B. Murray, R. J. Gorte, *Catal Letts.* **2018**, *148*, 1047-1054.
6. K. Salnikova, V. Matveeva, A. Bykov, G. Demidenko, I. Shkileva, E. Sulman, *ChemEng Trans.* **2018**, *70*, 379-384.
7. J. J. Musci, A. B. Merlo, M. L. Casella, *Catal. Today.* **2016**, *296,* 43-50.
8. C. Ramirez-Barria, M. Isaacs, K. Wilson, A. Guerrero-Ruiz, I. Rodríguez-Ramos, *Appl. Catal. A.* **2018**, *563,* 177-184.

9. R. M. Mironenko, O. B. Belskaya, T.I, Gulyaeva, A. I. Nizovskii, A. V. Kalinkin, V. I. Bukhtiyarov, A. V. Lavrenov, V. A. Likholobov, *Catal. Today*. **2015**, 249, 145-152.
10. C. Wang, Y. V. Kaneti, Y. Bando, J. Lin, C. Liu, J. Li, Y. Yamauchi, *Mater. Horiz.* **2018**, *5*, 394-407.
11. F. Yang, W. Li, Y. Zhanga, B. Tang, *Dalton Trans*. **2018**, *47*, 13657-13667.
12. Q. L. Zhua, P. Pachfulea, P. Strubelb, Z. Lia, R. Zouc, Z. Liud, S. Kaskelb, Q. Xu, *Energy Storage Materials*. **2018**, *13*, 72-79.
13. W. Xuan, R. Ramachandran, C. Zhao, F. Wang, *J Solid State Electrochem.* **2018**, *22*, 3873-388.
14. D. Banerjee, C. M. Simon, S. K. Elsaidi, M. Haranczyk, P. K. Thallapally, *Chem*. **2018,** *4*(3), 466-494.
15. L. Yang, X. Zeng, W. Wang, D. Cao, *Adv. Funct. Mater*. **2018**, *28*, 1704537
16. A. Aijaz, N. Fujiwara, Q. Xu, *J. Am. Chem. Soc*. **2014**, *136*(19), 6790-6793.
17. H. Zhang, J. Li, Q. Tan, L. Lu, Z. Wang, G. Wu, *Chem. Eur J.* **2018**, 24, 18137-18157.
18. Y. Zhan, L. Shen, C. Xu, W. Zhao, Y. Cao, L. Jiang, *CrystEng Comm*. **2018**, *20*(25), 3449-3454.
19. J. Zhou, Y. Dou, A. Zhou, L. Shu, Y. Chen, J. R. Li, ACS *Energy Lett*. **2018**, *3*(7), 1655-1661.
20. L. Zhaoqiang, Y. Longwei, *Energy Storage Materials*. **2018**, *14*, 367-375.
21. R. Wang, X. Sun, S. O. Chikh, D. Osadchii, F. Bai, F. Kapteijn, J. Gascon, *Appl. Mater. Interfaces*. **2018**, *10* (17), 14751-14758.
22. C. Young, R. R. Salunkhe, J. Tang, C. C. Hu, M. Shahabuddin, E. Yanmaz, M. Shahriar, A. Hossain, J. H. Kim, Y. Yamauchi, *Phys. Chem. Chem. Phys*. **2016**, *18*, 29308-29315.
23. L. Wan, E. Shamsaei, C. D. Easton, D. Yu, Y. Liang, X. Chen, Z. Abbasi, A. Akbari, X. Zhang, H. Wang, *Carbon*. **2018**, *121*, 330-336.
24. X. Liu, B. Zhang, B. Fei, X. Chen, J. Zhanga, X. Mu, *Faraday Discuss*. **2017**,*202*, 79-98.
25. M. A. Tike, V. V. Mahajani, *Ind. Eng. Chem. Res.* **2007**, *46*, 3275-3282.
26. Y. Soloveva, Y. V. Ioni, S. P. Gubin, *Mendeleev Commun*. **2016**, *26*, 38-39.
27. J. Zhang, X. Wang, D. Qin, Z. Xue, X. Lu, *Appl. Surf. Sci.* **2014**, 320, 73-82.
28. X. Wei, Y. Zhou, Y. Li, W. Shen, *RSC Adv*. **2015**, *5*, 66141-66146.

29. A. Sárkány, Z. Zsoldos, G. Stefler, J. W. Hightower, L. Guczi, *J. Catal*. **1995,** *157*, 179-189.
30. K. Shen, L. Chen, J. Long, W. Zhong, Y. Li, *ACS Catal*. **2015**, *5*, 5264-527.
31. G. Ma, C. Li, F. Liu, M. K. Majeed, Z. Feng, Y. Cui, J. Yang, Y. Qian, *Materials Today Energy*. **2018**, *10*, 241-248.
32. M. Savastano, P. A. Mascarós, C. Bazzicalupi, M. P. Clares, M. L. G. Salido, M. D. G. Valero, M. Inclán, A. Bianchi, E. G. España, R. L. Garzón, *J. Catal*. **2017,** *353*, 239-249.
33. Q. Qu, J. H. Zhang, J. Wang, Q. Y. Li, C. W. Xu, X. Lu, *Sci Rep*. **2017**, *7*, 41542.
34. M. A. Ghasemzadeh, Z. Elyasi, *Iran. j. catal.* **2017,** *7*(1), 75-83.
35. Y. Tuo, G. Liu, B. Dong, J. Zhou, A. Wang, J. Wang, R. Jin, H. Lv, Z. Dou, W. Huang, *Sci Rep*. **2015**, *5*, 13515
36. X. Zhang, Y. Niu, X. Meng, Y. Li, J. Zhao, *CrystEngComm.* **2013**, *15*, 8166-8172.
37. K. Song, Y. Lee, M. R. Jo, K. M. Nam, Y. M. Kang, *Nanotechnology*. **2012**, *23*, 505401.
38. A. Diallo, A. C. Beye, T. B. Doyle, E. Park, M.Maaza, *Green Chem Lett Rev.* **2015,** *8(3-4)*, 30-36.
39. C. W. Tang, C. B. Wang, S. H. Chien, *ThermochimicaActa*. **2008,** *473 (1-2)*, 68-73.
40. S. H. Cho, J. W. Jung, C. Kim, I. D. Kim, *Sci Rep*. **2017**, *7(1)*, 45105.
41. S. Bhogeswararao, D. Srinivas, *J. Catal.* **2015,** *327*, 65-77.
42. S. Sitthisa, T. Sooknoi, Y. Ma, P. B. Balbuena, D. E. Resasco, *J. Catal*. **2011,** *277*, 1-13.
43. M. D. Argyle, C. H. Bartholomew, *Catalysts.* **2015**, *5*, 145-269.
44. J. V.Doorn, J.A. Moulijn, *Catal. Today*. **1990,** *7*, 257-266.

Graphical Abstract:

Metal-Organic-Framework Derived Co-Pd Catalyst is Preferred over Fe-Pd for Reductive Upgrading of Furfural to Tetrahydrofurfuryl alcohol

Saikiran Pendem, Bolla Srinivasa Rao, David J. Morgan, Digambar B. Shinde, ZhipingLai, Nakka Lingaiah, and John Mondal*

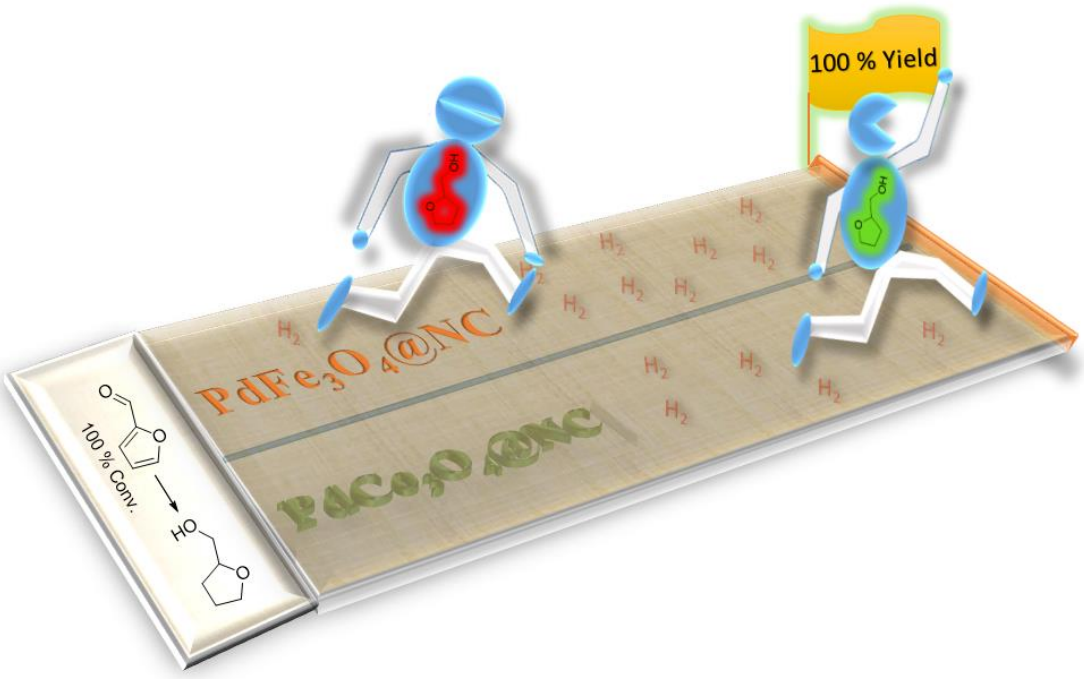
100 % Yield
PdFe3O4@NC
PdCo3O4@NC
100 % Conv.